IEEE Photonics Journal
An IEEE Photonics Society Publication

Open Access

Grating Couplers Integrated on Mach–Zehnder Interferometric Biosensors Operating in the Visible Range

Volume 5, Number 2, April 2013

Daphné Duval
Johann Osmond
Stefania Dante
Carlos Domínguez
Laura M. Lechuga

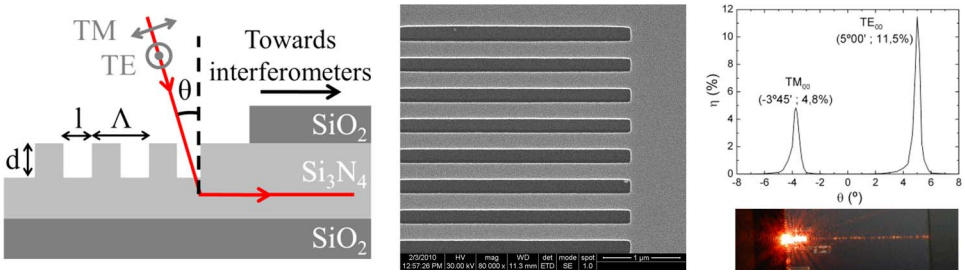

DOI: 10.1109/JPHOT.2013.2251873
1943-0655/$31.00 ©2013 IEEE

IEEE photonics SOCIETY

IEEE

Grating Couplers Integrated on Mach–Zehnder Interferometric Biosensors Operating in the Visible Range

Daphné Duval,[1] Johann Osmond,[2] Stefania Dante,[1] Carlos Domínguez,[3] and Laura M. Lechuga[1]

[1]Nanobiosensors and Bioanalytical Applications Group, CIN2 (CSIC) and CIBER-BBN, 08193 Bellaterra (Barcelona), Spain
[2]Institute of Photonic Sciences, ICFO, 08860 Castelldefels (Barcelona), Spain
[3]Institute of Microelectronics of Barcelona, IMB-CNM (CSIC), 08193 Bellaterra (Barcelona), Spain

DOI: 10.1109/JPHOT.2013.2251873

Manuscript received January 14, 2013; revised February 28, 2013; accepted February 28, 2013. Date of publication March 8, 2013; date of current version March 22, 2013. This work was supported in part by the M. Botin foundation and in part by the Spanish ministry of economy and competitiveness through Grant NOLA (TEC2009-09380). The work of S. Dante was supported by the "Programa de Formación de Profesorado Universitario (FPU)" of the "Ministerio de Educación" of Spain. Corresponding author: L. M. Lechuga (e-mail: laura.lechuga@cin2.es).

Abstract: We present the design, fabrication, and characterization of submicronic grating couplers integrated on Si_3N_4 rib waveguide Mach–Zehnder interferometers (MZIs) for biosensing applications working in the visible spectral range for both TE and TM polarizations. Depending on the waveguide structure, a maximum of 11.5% of coupling efficiency has been experimentally obtained at 658 nm, while a limit of detection of 1.6×10^{-7} in refractive index unit is achieved for the biosensor. These results represent an important milestone toward the achievement of a truly portable and multiplexed point-of-care platform using the integrated MZI sensor.

Index Terms: Gratings, biosensors, integrated optics (IO), interferometry.

1. Introduction

Diffraction gratings, which are a fundamental building block of integrated optics (IO), have been extensively studied over the last decades, and a solid platform for their modeling and fabrication has been created [1]–[5]. They find applications as passive components such as reflectors [2] or wavelength filters [6]. They are also widely employed as couplers from fiber or free-space light to thin-film optical waveguides (and vice versa) [7], [8] as they provide better integration and better alignment tolerance than other usual techniques such as end-fire or prism-assisted coupling methods. Grating couplers can moreover be fabricated at wafer level and do not require polishing steps. Due to these advantages, they are employed as a reliable coupling technology in the photonics industry [9], [10].

On the other side, IO biosensors based on the evanescent wave detection principle have been revealed over the last years as the most promising transducers for achieving a fully operative lab-on-a-chip (LOC) platform with on-chip detection as they offer high sensitivity, mechanical stability, miniaturization, and the possibility of mass production [11]. They also present the advantages inherent to optical readouts, i.e., noninvasive and nondestructive nature, absence of risk of electrical shocks or explosions, and immunity to electromagnetic interferences. Among the different IO sensors described in the literature or commercially available, the ring resonators [limit of detection (LOD) of 7.6×10^{-7} refractive index unit (RIU) in bulk] have positioned themselves as one of the most

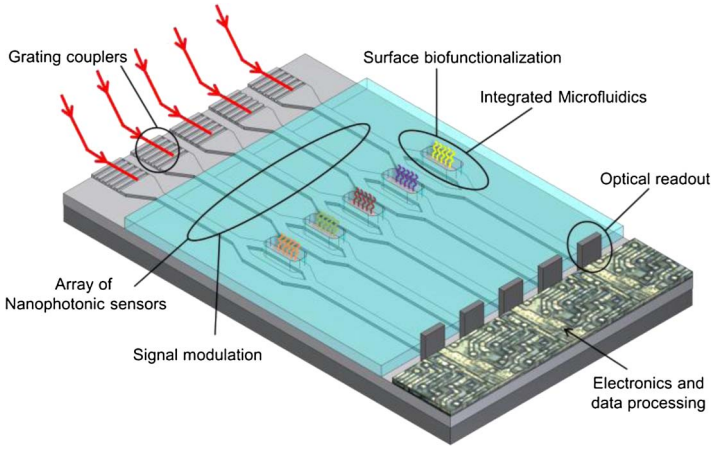

Fig. 1. Scheme of an envisioned LOC platform based on MZI transducers.

competitive IO biosensors [12]. It is also worthwhile mentioning the wavelength interrogated optical sensors (WIOS) based on gratings (LOD: 2.5×10^{-6} RIU) [13], photonic crystals (LOD: 1.6×10^{-4} RIU) [14], Young interferometers (LOD: 6×10^{-8} RIU) [15], or Mach–Zehnder interferometers (MZI; LOD: 1×10^{-7} RIU) [16]. An extensive discussion about IO biosensors can be found in [11].

However, the way to reliably couple light into the submicronic cross section of the IO sensing waveguides is still challenging. It has to be taken into account that the future LOC platform should be portable and that the photonic chip would have to be frequently replaced in the platform. For these reasons, high alignment tolerance between the input beam and the photonic chip is a mandatory requirement, and this can only be provided by grating couplers. This tolerance in the alignment will also facilitate the implementation of a multiplexed platform. That is the reason why grating couplers appear as the most appropriate coupling solution for the implementation of LOC platforms based on IO biosensors. Such a LOC device should incorporate on the same platform the photonic sensors in a multiplexed configuration, the microfluidic cell network, the light source and the photodetectors, robust biofunctionalization protocol for the biological receptors, and the processing electronics, including a final packaging with the required firmware and software (see Fig. 1).

Grating couplers have already been successfully employed and integrated on IO biosensors operating in the near infrared [17]–[20], and the biosensing capabilities of these systems have been demonstrated [21]–[23]. But apart from gratings used as WIOS [13], [24]–[26], grating couplers integrated with IO biosensors in the visible range have scarcely been investigated for biosensing applications [27]. This difference can be explained by the fact that grating couplers have been first developed for telecommunication applications, operating in wavelengths in the near-infrared range with grating periods in the order of 1 μm [7]. But due to the lack of applications in the visible range, gratings for visible wavelengths have not been extensively studied. Moreover, their fabrication is challenging as they request periods below 500 nm [3], [28]; as conventional UV lithography is unsuitable for fabrication of submicronic patterns, alternative fabrication processes such as electron-beam lithography (EBL), nanoimprint lithography, deep-UV lithography, optical holography, or focused ion beam milling have to be foreseen.

IO biosensors working in the visible range have clear advantages as compared to their counterparts operating in the infrared range. Most of the biomolecules employed are nonabsorbent in the visible, avoiding any damage or light absorption. In addition, optical setups working in the visible range are easier to implement as the light beam can be seen at naked eye and the light sources, photodetectors, and other optical components are rather low-cost when compared with the ones used for infrared applications; for example, they usually employ an expensive tunable laser.

Therefore, there is a strong need to achieve efficient grating couplers operating in the visible range. However, while most works are focused on designing grating couplers with the highest

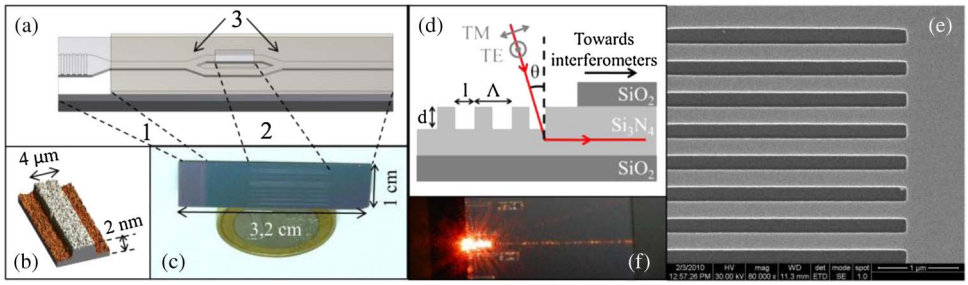

Fig. 2. (a) Scheme of a MZI sensor with 1: the grating window; 2: the sensing area and 3: the Y-junctions. (b) AFM image of the rib. (c) Photograph of a chip of 10 × 32 mm^2 containing 9 MZI and 24 waveguides. (d) Scheme and parameters of a grating coupler with a rectangular section profile. (e) SEM image of a 400 nm-period grating. (f) Photograph of device F1.1, highlighting the excited grating and the light propagating in the waveguide.

coupling efficiency without any particular constraint, the design of gratings integrated with visible IO biosensors is conditioned by the sensing capabilities of the device. Indeed, grating couplers with high coupling efficiency usually present complex layer structures, including for instance multilayer bottom reflectors [5], [29]. For biosensing applications, this would not only increase the fabrication complexity of the whole structure but, above all, would drastically affect the biosensor sensitivity.

Taking into account the above considerations, we have designed, fabricated, and integrated grating couplers working in the visible range within micro-MZI biosensors using silicon technology. We have validated the full development by demonstrating the sensing capabilities of the device with the final aim of implementing a complete LOC platform working at 658 nm in TE or TM polarization.

2. Device Design and Fabrication

In the integrated MZI configuration [see Fig. 2(a)], a first Y-junction splits the guided light into two arms, i.e., the sensing and the reference arms. After a certain distance, the two signals are recombined into an output waveguide via a second Y-junction, producing the interference of both beams. The interferometers were fabricated using standard silicon technologies in clean room facilities and were based on a rib waveguide configuration. Si_3N_4 deposited by low-pressure chemical vapor deposition was chosen as the core material for the rib waveguides as it offers very low loss in the entire optical range and shows a sufficiently high refractive index ($n_{Si_3N_4} = 2.00$ at 658 nm), enabling high surface sensitivity, as well as a precise control of light path and modal behavior [30]–[33]. Two families of MZI were studied (see Table 1). The first family had a core thickness $h_{Si_3N_4}$ of 200 nm and a rib width w_{rib} of 4 μm (devices named F1.X), and the second one had a core thickness of 250 nm and a rib width of 2.5 μm (devices named F2.X). In both cases, the rib height had to be below 2 nm [see Fig. 2(b)] in order to maximize the sensor sensitivity and ensure lateral single-mode behavior, in both TE and TM polarizations [32], [33]. Bottom and top claddings were constituted of silicon dioxide layers, and for biosensing applications, a portion of the top cladding was removed to define the sensing area $(15 \times 0.05\ \text{mm}^2)$, where the evanescent field can probe the external medium. A portion of the cladding was also removed at the input of the chip to define the grating window. The final chip dimensions are 32 × 10 mm^2, and it contains 9 MZIs and 24 waveguides [see Fig. 2(c)].

In order to increase the coupling efficiency, we previously defined at the entrance of the grating window a tapered waveguide with initial widths w_{taper} of 20, 30, or 50 μm that linearly reduces until reaching the interferometer waveguide widths (2.5 or 4 μm). The grating couplers were then fabricated onto the tapered region of the waveguide.

The resonant coupling between the guided mode and a diffraction order of the grating is governed by the phase matching condition

$$\sin\theta = n_{eff} + m\frac{\lambda}{\Lambda} \tag{1}$$

TABLE 1

Parameters of the devices for family 1 (F1.X) and family 2 (F2.X) with $h_{Si_3N_4}$ the MZI core thickness, w_{rib} the MZI rib width, w_{taper} the initial taper width, α the correction coefficient, Λ the grating period and θ_{th} the theoretical excitation angle of the grating for both TE_{00} and TM_{00} modes at $\lambda = 658$ nm

h_{Si3N4} (nm)	w_{rib} (μm)	w_{taper} (μm)	α	Λ (nm)	θ_{th} TE_{00}	θ_{th} TM_{00}	Device name
200	4	30	0.29	400	6.7°	-1.3°	F1.1
		20	0.20	450	17.4°	9.2°	F1.2
250	2.5	50	0.53	400	9.9°	4.2°	F2.1
				425	15.6°	9.8°	F2.2

with θ as the incident angle of light, n_{eff} as the effective refractive index of the guided mode, m as the diffraction order (here $m = -1$), λ as the wavelength in air, and Λ as the grating period. The effective refractive index, which depends on the material and dimensions of the waveguide, is calculated for each structure by the effective index method.

The gratings were designed taking into account previous studies [1], [2], [29] but without modifying the layer structure of the MZI, which has already been optimized for biosensing applications [32]. Equation (1) was used to set the incident angles ranging from 5° to 10°, which should enable an efficient coupling. Moreover, it is an important requirement for the implementation of a portable platform in which all the different components have to be integrated together in a minimal space without disturbing each other. Taking into account these considerations, the grating periods were set between 400 and 450 nm with a duty cycle of 0.5. The duty cycle is defined as l/Λ, where l is the groove width of the grating. Regarding the groove depth d, partially etched gratings are preferred as they allow a reduction of the diffraction efficiency of the grating and, therefore, an increase of the coupling efficiency into the waveguide. We set a groove depth of 50 nm according to a preliminary study performed for depths ranging from 25 to 50 nm. Grating parameters are represented in Fig. 2(d).

The gratings were directly written on the Si_3N_4 tapered waveguide. A poly(methyl methacrylate) resist layer was first patterned with electron beam lithography. The gratings were then transferred to Si_3N_4 of the desired etch depth of 50 nm by reactive ion etching using CHF_3/O_2 gas chemistry. For family 1, gratings with periods of 400 nm (device F1.1) and 450 nm (device F1.2) were investigated for coupling of the TE_{00} and TM_{00} modes, respectively. For family 2, the studied periods were 400 nm (device F2.1) and 425 nm (device F2.2) for TE_{00} and TM_{00} modes, respectively. All the gratings have a length of 100 μm and a width equal to the taper width (20 to 50 μm). Parameters and names of the devices, as well as the theoretical excitation angles, are summarized in Table 1.

Fig. 2(e) shows a scanning electron microscope (SEM) image of a 400-nm-period grating, highlighting the high quality of the grating. In particular, we can note the excellent definition of the grooves.

3. Optical Characterization

To measure the coupling efficiency of the gratings, a light beam from a fiber pigtailed Fabry–Perot laser diode was coupled into the MZI chip, mounted on a rotation stage, by focusing the incident beam on the gratings with a fiber coupling lens pair. Two laser diodes have been used, one emitting at 658 nm ($P_0 = 40$ mW) and one at 635 nm ($P_0 = 3.5$ mW). In both cases, the optical fiber was placed in such a way that the incident beam was polarized at 45° and a polarizer was intercalated between the lens and the grating to select the proper polarization (TE or TM). The coupled light propagated into the waveguide until the edge of the chip where it was collected and monitored by a silicon photodiode connected to a current amplifier. Fig. 2(f) shows the excited grating and the coupled light propagating in a waveguide of device F1.1.

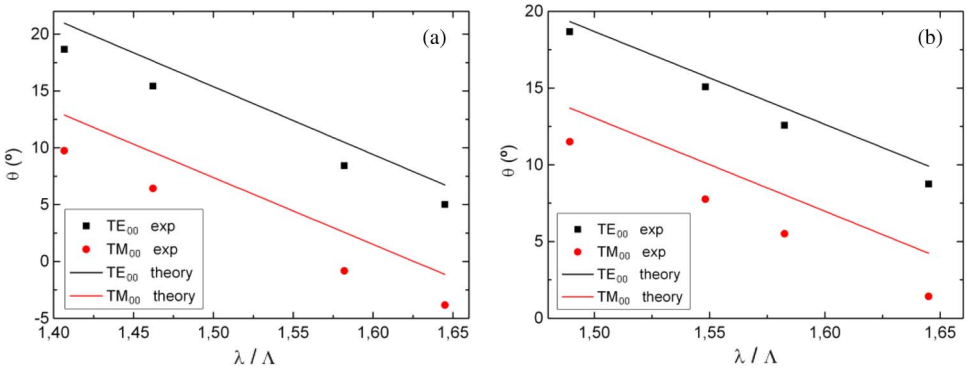

Fig. 3. Dispersion relation: comparison between experimental and theoretical results for all the devices of (a) family 1 and (b) family 2.

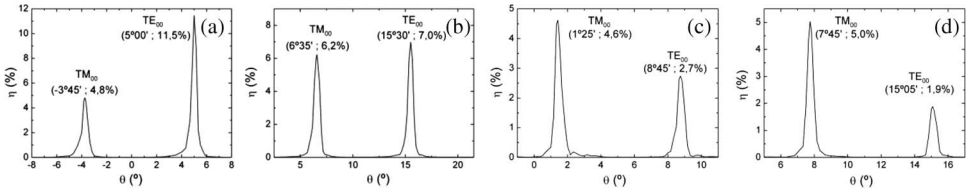

Fig. 4. Coupling efficiency at 658 nm as a function of the incidence angle for devices (a) F1.1, (b) F1.2, (c) F2.1, and (d) F2.2.

As a first step, we determined the excitation angles of each device for two different visible wavelengths (635 and 658 nm), and we compared them with the theoretical values calculated from (1). Results for all the devices of families 1 and 2 are presented in Fig. 3(a) and (b), respectively. First of all, we observed that the experimental results are in good agreement with the theory: differences between theoretical and experimental results of 1°30′ and of 2°45′ are observed on average for TE_{00} and TM_{00} modes, respectively. Moreover, we observed a fine reproducibility of the results: the average deviation of the excitation angle measured on 12 different gratings with the same nominal parameters is of only 0°15′.

The coupling efficiency is defined as

$$\eta = \alpha \frac{I_g}{I_0} \tag{2}$$

with I_g as the output intensity measured by the photodiode, I_0 as the incident intensity at the output of the laser and α as the correction coefficient defined by the contact area between the incident beam and the grating coupler (see Table 1). This expression is valid as long as propagation losses are negligible, which is the case when working with Si_3N_4 rib waveguides (for a MZI with a core of 200 nm, the propagation losses are 0.19 dB/cm and 0.22 dB/cm for TE_{00} and TM_{00} modes, respectively [34]).

Fig. 4 shows the coupling efficiency evaluated at 658 nm, the wavelength of our future LOC platform, as a function of the incident angle for the four studied devices. As can be observed in Fig. 4(a), device F1.1 allows a very efficient coupling of 11.5% at 5° for TE_{00} mode. In TM polarization, device F1.2 enables a coupling efficiency of 6.2% at 6°35′ [see Fig. 4(b)]. For the MZI with a 250 nm-core, a coupling efficiency of 2.7% at 8°45′ is obtained in TE polarization for the device F2.1 [see Fig. 4(c)], while a coupling efficiency of 5% has been achieved at 7°45′ for the TM_{00} mode for the device F2.2 [see Fig. 4(d)]. We can observe that the coupling efficiency is weaker for the devices of family 2, particularly for the TE_{00} mode. This could be explained by the

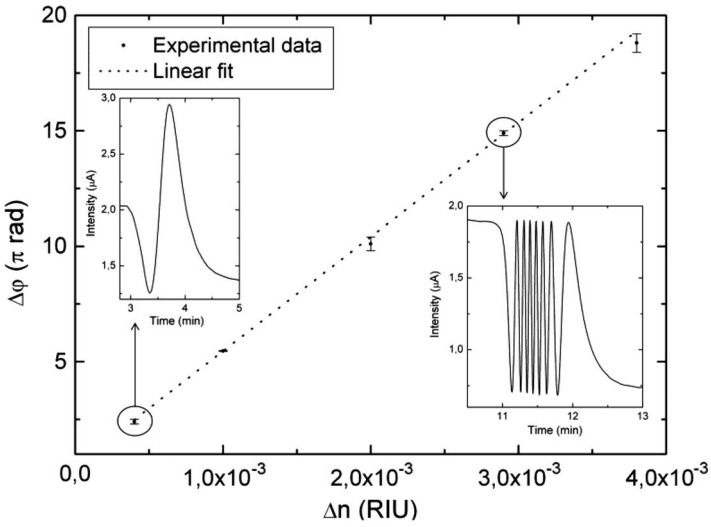

Fig. 5. Calibration curve of device F2.2 in TM polarization. Insets: sensor response to the injection of (left) HCl 0.03 M and of (right) HCl 0.3 M.

differences in the geometric configuration of the two families (taper width, waveguide width, and core thickness).

The comparison of these results with the ones obtained by the end-fire method is not straightforward due to the very small cross section of our waveguides. Indeed, for the end-fire method, the correction coefficient α has much more influence on the coupling efficiency than for the grating coupler method. However, we can directly compare the output intensity: for the same laser input intensity, the waveguide output intensity is between five and ten times higher with the grating coupler method than with the end-fire method. This clearly demonstrates that, for waveguides of such dimensions, the grating coupler method results in better coupling than the end-fire method.

We studied the influence of alignment on the coupling efficiency on 18 different gratings, in both TE and TM polarizations. The angle tolerance ranges from $0°25'$ to $0°45'$ at -3 dB. The exact lateral position tolerance depends on the taper size, but it is in the order of a few tens of microns. These values clearly support the adoption of grating couplers as the best in-coupling choice for the achievement of a portable device.

4. Sensing Validation

To evaluate the sensing capabilities of the integrated MZI with the grating couplers incorporated, the chip was placed on a XYZ translation stage (NanoMax, Thorlabs) with the fiber pigtailed laser diode mounted on a rotation stage above the chip. A microfluidic header made of a PDMS flow cell encapsulated in a PMMA housing was mounted onto the chip to control the liquid flow.

The sensitivity of the device was evaluated by measuring the phase changes $\Delta\varphi$ induced by refractive index variation Δn in the sensing area. Different concentrations of HCl (from 0.03 to 0.4 M) were injected $(\mathrm{V} = 250\ \mu\mathrm{l})$ through a syringe pump with running water (milli-Q grade) as buffer. The refractive indices of the solutions were previously determined with an ABBE refractometer, and the corresponding phase change $\Delta\varphi$ was deduced from the interference pattern at the MZI output. As a result of the evaluation of the different concentrations, Fig. 5 shows the calibration curve corresponding to device F2.2 for TM polarization [$\theta = 7°45'$, $\eta = 5.0\%$; see Fig. 4(d)]. Each detection was repeated three times, and the corresponding standard deviations are included in Fig. 5 as error bars. A linear fit of the experimental data results in a sensitivity S of $4950 \times \pi$ rad/RIU, with $R^2 = 0.999$. As the noise-to-signal ratio of our system is of $2.7 \times 10^{-4} \times \pi$ rad, the phase resolution $\Delta\varphi_{\mathrm{min}}$ of the sensor, defined as three times the noise-to-signal ratio, is of $8.1 \times 10^{-4} \times \pi$ rad. The LOD of our sensor in terms of RIUs is given by $\Delta n_{\mathrm{min}} = \Delta\varphi_{\mathrm{min}}/S$, resulting in $\Delta n_{\mathrm{min}} = 1.6 \times 10^{-7}$ RIU. This LOD,

obtained with a low-cost laser diode and a grating with a coupling efficiency of only 5.0%, is comparable with the LOD of 1.0×10^{-7} RIU demonstrated in our previous study using a HeNe laser and end-fire coupling [16].

5. Conclusion

We have designed, fabricated, and characterized efficient grating couplers incorporated on integrated Si_3N_4 MZI biosensors working in the visible spectral range for both TE and TM polarization. Although higher experimental coupling efficiencies have been reported for grating coupler integrated with single-mode waveguides, a quite good coupling efficiency (up to 11.5%) has been obtained, taking into account that most of the parameters have been fixed to maintain the high surface sensitivity of the MZI device. We have demonstrated a LOD of $\Delta n_{\text{min}} = 1.6 \times 10^{-7}$ RIU, which is comparable with the state-of-the-art IO biosensors [11]. We have proven that an excellent sensitivity can be achieved by incorporating the grating couplers as a way to efficiently couple the light into the rib waveguides. This result is an important milestone toward our final objective of assembling a portable LOC platform with multiplexing capabilities while maintaining the sensitivity level for the label-free detection required in the clinical diagnostic field. Next steps include the implementation of the multiplexed biosensors taking advantage of the grating couplers to form waveguide arrays, as well as the evaluation of the robustness of the LOC device in field condition.

References

[1] J. H. Harris, R. K. Winn, and D. G. Dalgoutte, "Theory and design of periodic couplers," *Appl. Opt.*, vol. 11, no. 10, pp. 2234–2241, Oct. 1972.

[2] T. Tamir and S. Peng, "Analysis and design of grating couplers," *Appl. Phys. A, Mater.*, vol. 14, no. 3, pp. 235–254, Nov. 1977.

[3] J. C. Brazas and L. Li, "Analysis of input-grating couplers having finite lengths," *Appl. Opt.*, vol. 34, no. 19, pp. 3786–3792, Jul. 1995.

[4] O. Parriaux, V. A. Sychugov, and A. V. Tishchenko, "Coupling gratings as waveguide functional elements," *Pure Appl. Opt.*, vol. 5, no. 4, pp. 453–470, Jul. 1996.

[5] D. Taillaert, F. Van Laere, M. Ayre, W. Bogaerts, D. Van Thourhout, P. Bienstman, and R. Baets, "Grating couplers for coupling between optical fibers and nanophotonic waveguides," *Jpn. J. Appl. Phys.*, vol. 45, no. 8A, pp. 6071–6077, Aug. 2006.

[6] J. Hübner, D. Zauner, and M. Kristensen, "Strong sampled Bragg gratings for WDM applications," *IEEE Photon. Technol. Lett.*, vol. 10, no. 4, pp. 552–554, Apr. 1998.

[7] G. Maire, L. Vivien, G. Sattler, A. Kazmierczak, B. Sanchez, K. B. Gylfason, A. Griol, D. Marris-Morini, E. Cassan, D. Giannone, H. Sohlstrom, and D. Hill, "High efficiency silicon nitride surface grating couplers," *Opt. Exp.*, vol. 16, no. 1, pp. 328–333, Jan. 2008.

[8] M. Antelius, K. B. Gylfason, and H. Sohlstrom, "An apodized SOI waveguide-to-fiber surface grating coupler for single lithography silicon photonics," *Opt. Exp.*, vol. 19, no. 4, pp. 3592–3598, Feb. 2011.

[9] C. Gunn, "CMOS photonics for high-speed interconnects," *IEEE Micro*, vol. 26, no. 2, pp. 58–66, Mar./Apr. 2006.

[10] L. C. Gunn, T. J. Pinguet, and M. J. Rattier, "Optical waveguide grating coupler incorporating reflective optical elements and anti-reflection elements," U.S. Patent 7 184 625, Feb. 27, 2007.

[11] M. C. Estevez, M. Alvarez, and L. M. Lechuga, "Integrated optical devices for lab-on-a-chip biosensing applications," *Laser Photon. Rev.*, vol. 6, no. 4, pp. 463–487, Jul. 2012.

[12] M. Iqbal, M. A. Gleeson, B. Spaugh, F. Tybor, W. G. Gunn, M. Hochberg, T. Baehr-Jones, R. C. Bailey, and L. C. Gunn, "Label-free biosensor arrays based on silicon ring resonators and high-speed optical scanning instrumentation," *IEEE J. Sel. Topics Quantum Electron.*, vol. 16, no. 3, pp. 654–661, May/Jun. 2010.

[13] K. Cottier, M. Wiki, G. Voirin, H. Gao, and R. E. Kunz, "Label-free highly sensitive detection of (small) molecules by wavelength interrogation of integrated optical chips," *Sens. Actuators B, Chem.*, vol. 91, no. 1–3, pp. 241–251, Jun. 2003.

[14] J. García-Rupérez, V. Toccafondo, M. J. Bañuls, J. G. Castelló, A. Griol, S. Peransi-Llopis, and Á. Maquieira, "Label-free antibody detection using band edge fringes in SOI planar photonic crystal waveguides in the slow-light regime," *Opt. Exp.*, vol. 18, no. 23, pp. 24 276–24 286, Nov. 2010.

[15] A. Ymeti, J. S. Kanger, J. Greve, G. A. J. Besselink, P. V. Lambeck, R. Wijn, and R. G. Heideman, "Integration of microfluidics with a four-channel integrated optical Young interferometer immunosensor," *Biosens. Bioelectron.*, vol. 20, no. 7, pp. 1417–1421, Jan. 2005.

[16] K. E. Zinoviev, L. G. Carrascosa, J. Sánchez del Río, B. Sepúlveda, C. Domínguez, and L. M. Lechuga, "Silicon photonic biosensors for lab-on-a-chip applications," *Adv. Opt. Technol.*, vol. 2008, pp. 383927-1–383927-6, 2008.

[17] R. Bruck and R. Hainberger, "Polymer waveguide based biosensor," in *Proc. SPIE*, May 2008, vol. 7138, pp. 71380N-1–71380N-7.

[18] A. Densmore, D. X. Xu, P. Cheben, M. Vachon, S. Janz, R. Ma, D. Bedard, Y. Li, G. Lopinski, A. Delâge, J. H. Schmid, R. Halir, and I. Molina-Fernández, "Integration of vertical grating couplers and microfluidic channels with silicon photonic wire biosensor arrays," in *Proc. IEEE Sens.*, Nov. 2010, pp. 1550–1553.

[19] L. Wang, Y. Li, M. Garcia Porcel, D. Vermeulen, X. Han, J. Wang, X. Jian, M. Zhao, and G. Morthier, "Grating couplers in polymer with a thin Si3N4 layer embedded," in *Proc. SPIE*, Feb. 2012, vol. 8258, pp. 825817-1–825817-7.
[20] L. Wang, J. Ren, X. Han, T. Claes, X. Jian, P. Bienstman, R. Baets, M. Zhao, and G. Morthier, "A label-free optical biosensor built on a low-cost polymer platform," *IEEE Photon. J.*, vol. 4, no. 3, pp. 920–930, Jun. 2012.
[21] C. F. Carlborg, K. B. Gylfason, A. Kazmierczak, F. Dortu, M. J. Banuls Polo, A. Maquieira Catala, G. M. Kresbach, H. Sohlstrom, T. Moh, L. Vivien, J. Popplewell, G. Ronan, C. A. Barrios, G. Stemme, and W. van der Wijngaart, "A packaged optical slot-waveguide ring resonator sensor array for multiplex label-free assays in labs-on-chips," *Lab Chip*, vol. 10, no. 3, pp. 281–290, Feb. 2010.
[22] R. Bruck, E. Melnika, P. Muellner, R. Hainberger, and M. Lammerhofer, "Integrated polymer-based Mach–Zehnder interferometer label-free streptavidin biosensor compatible with injection molding," *Biosens. Bioelectron.*, vol. 26, no. 9, pp. 3832–3837, May 2011.
[23] M. K. Park, J. S. Kee, J. Y. Quah, V. Netto, J. Song, Q. Fang, E. M. La Fosse, and G.-Q. Lo, "Label-free aptamer sensor based on silicon microring resonators," *Sens. Actuators B, Chem.*, vol. 176, pp. 552–559, Jan. 2013.
[24] G. Suárez, Y.-H. Jin, J. Auerswald, S. Berchtold, H. F. Knapp, J.-M. Diserens, Y. Leterrier, J.-A. E. Manson, and G. Voirin, "Lab-on-a-chip for multiplexed biosensing of residual antibiotics in milk," *Lab Chip*, vol. 9, no. 11, pp. 1625–1630, Jun. 2009.
[25] N. Darwish, D. Caballero, M. Moreno, A. Errachid, and J. Samitier, "Multi-analytic grating coupler biosensor for differential binding analysis," *Sens. Actuators B, Chem.*, vol. 144, no. 2, pp. 413–417, Feb. 2010.
[26] P. Kozma, A. Hámori, S. Kurunczi, K. Cottier, and R. Horvath, "Grating coupled optical waveguide interferometer for label-free biosensing," *Sens. Actuators B, Chem.*, vol. 155, no. 2, pp. 446–450, Jul. 2011.
[27] L. U. Kempen and R. E. Kunz, "Replicated Mach–Zehnder interferometers with focusing grating couplers for sensing applications," *Sens. Actuators B, Chem.*, vol. 39, no. 1–3, pp. 295–299, Mar./Apr. 1997.
[28] K. Zinoviev, C. Dominguez, and A. Vilà, "Diffraction grating couplers milled in Si3N4 rib waveguides with a focused ion beam," *Opt. Exp.*, vol. 13, no. 21, pp. 8618–8624, Oct. 2005.
[29] D. Taillaert, W. Bogaerts, P. Bienstman, T. F. Krauss, P. Van Daele, I. Moerman, S. Verstuyft, K. De Mesel, and R. Baets, "An out-of-plane grating coupler for efficient butt-coupling between compact planar waveguides and single-mode fibers," *IEEE J. Quantum Electron.*, vol. 38, no. 7, pp. 949–955, Jul. 2002.
[30] W. Lukosz, "Principles and sensitivities of integrated optical and surface plasmon sensors for direct affinity sensing and immunosensing," *Biosens. Bioelectron.*, vol. 6, no. 3, pp. 215–225, 1991.
[31] E. F. Schipper, A. M. Brugman, C. Dominguez, L. M. Lechuga, R. P. H. Kooyman, and J. Greve, "The realization of an integrated Mach–Zehnder waveguide immunosensor in silicon technology," *Sens. Actuators B, Chem.*, vol. 40, no. 2/3, pp. 147–153, May 1997.
[32] F. Prieto, B. Sepúlveda, A. Calle, A. Llobera, C. Domínguez, A. Abad, A. Montoya, and L. M. Lechuga, "An integrated optical interferometric nanodevice based on silicon technology for biosensor applications," *Nanotechnology*, vol. 14, no. 8, pp. 907–912, Aug. 2003.
[33] B. Sepulveda, J. S. del Rio, M. Moreno, F. J. Blanco, K. Mayora, C. Dominguez, and L. M. Lechuga, "Optical biosensor microsystems based on the integration of highly sensitive Mach–Zehnder interferometer devices," *J. Opt. A, Pure Appl. Op.*, vol. 8, no. 7, pp. S561–S566, Jul. 2006.
[34] J. Sánchez del Río, "Desarrollo de un biosensor fotónico de alta sensibilidad basado en interferómetros Mach–Zehnder integrados en tecnología microelectrónica de silicio," Ph.D. dissertation, Facultad de Ciencias, Univ. Autónoma de Madrid, Madrid, Spain, 2004.